Supporting Information

Direction-aware and Ultrafast Self-healing Dual Network Hydrogel for Flexible Electronic Skin Strain Sensor

Wenwu Peng,[a] Lu Han,[a] Hailong Huang,[a] Xiaoyang Xuan,[b] Guodong Pan,[a] Lijia Wan,[a] Ting Lu,[a] Min Xu,*[a] and Likun Pan*[a]

[a] Shanghai Key Laboratory of Magnetic Resonance, School of Physics and Electronic Science, East China Normal University, Shanghai 200241, China.

[b] Department of Physics, School of Science, East China University of Science and Technology, Shanghai 200237, China.

*Email: lkpan@phy.ecnu.edu.cn (Likun Pan); xumin@phy.ecnu.edu.cn (Min Xu)

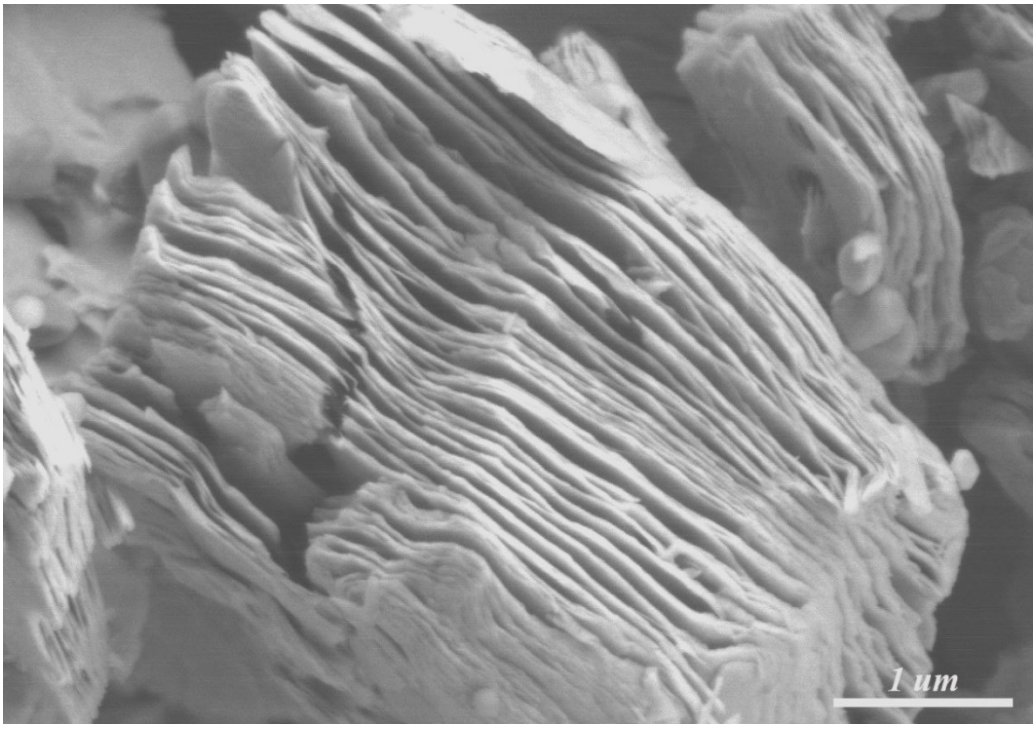

Figure S1. SEM image of MXene.

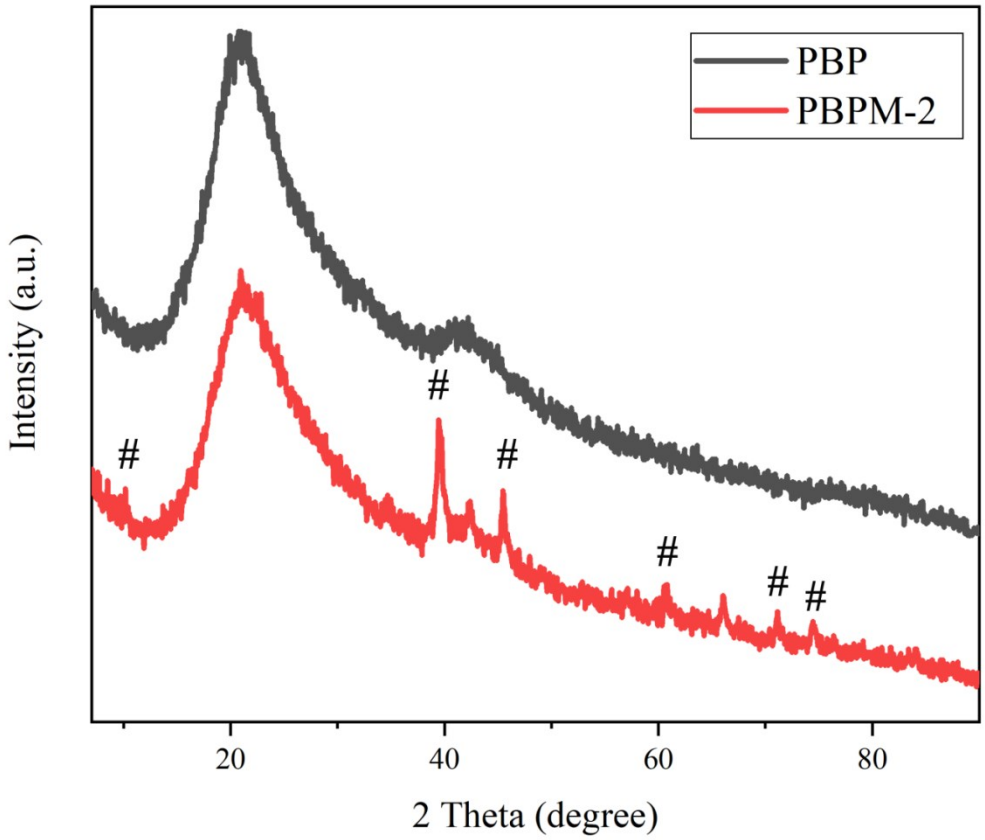

Figure S2. XRD patterns of the PBP and PBPM-2 hydrogel (# represents several new peaks in the XRD pattern of PBPM-2 compared with PBP).

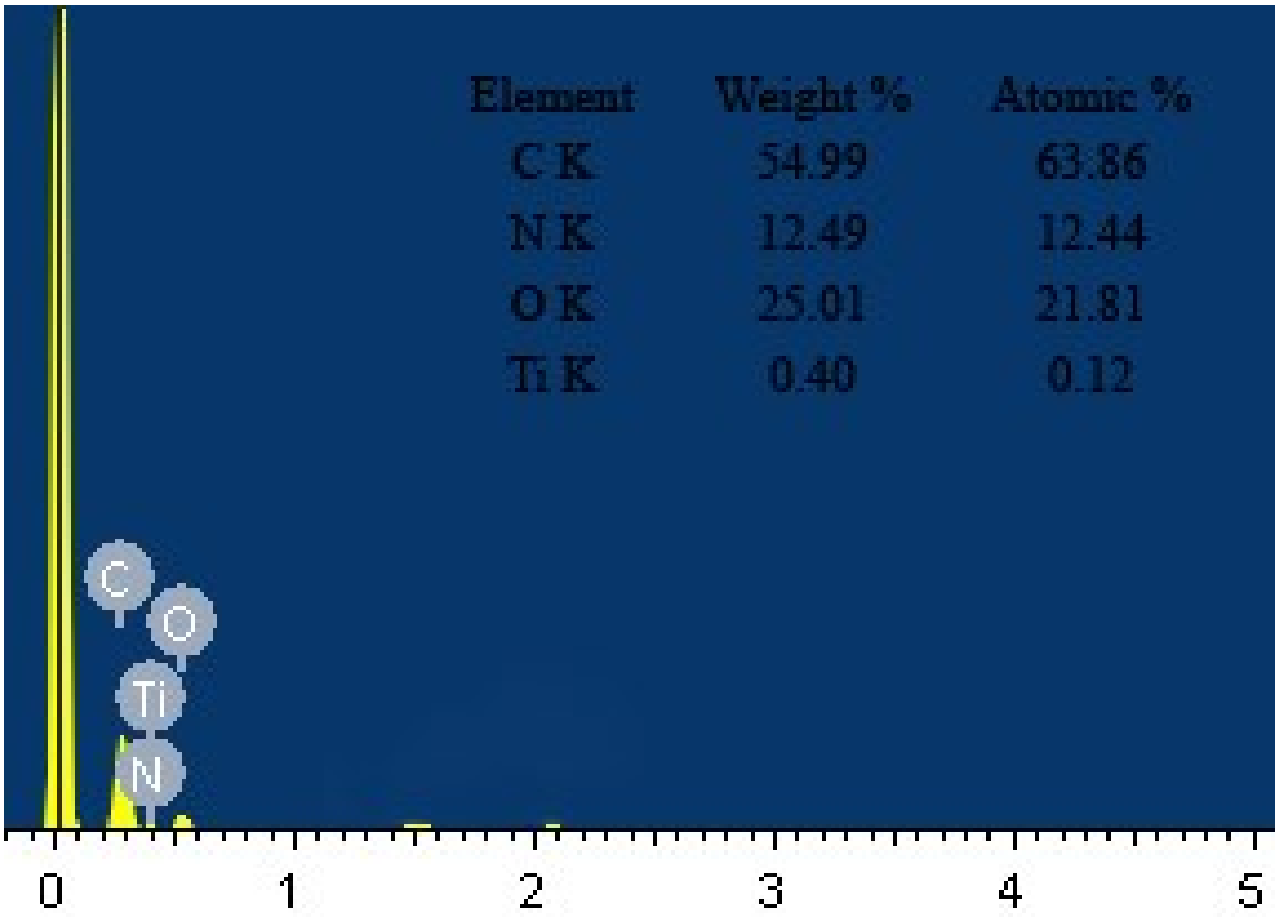

Figure S3. EDS spectrum of the PBPM-2 hydrogel.

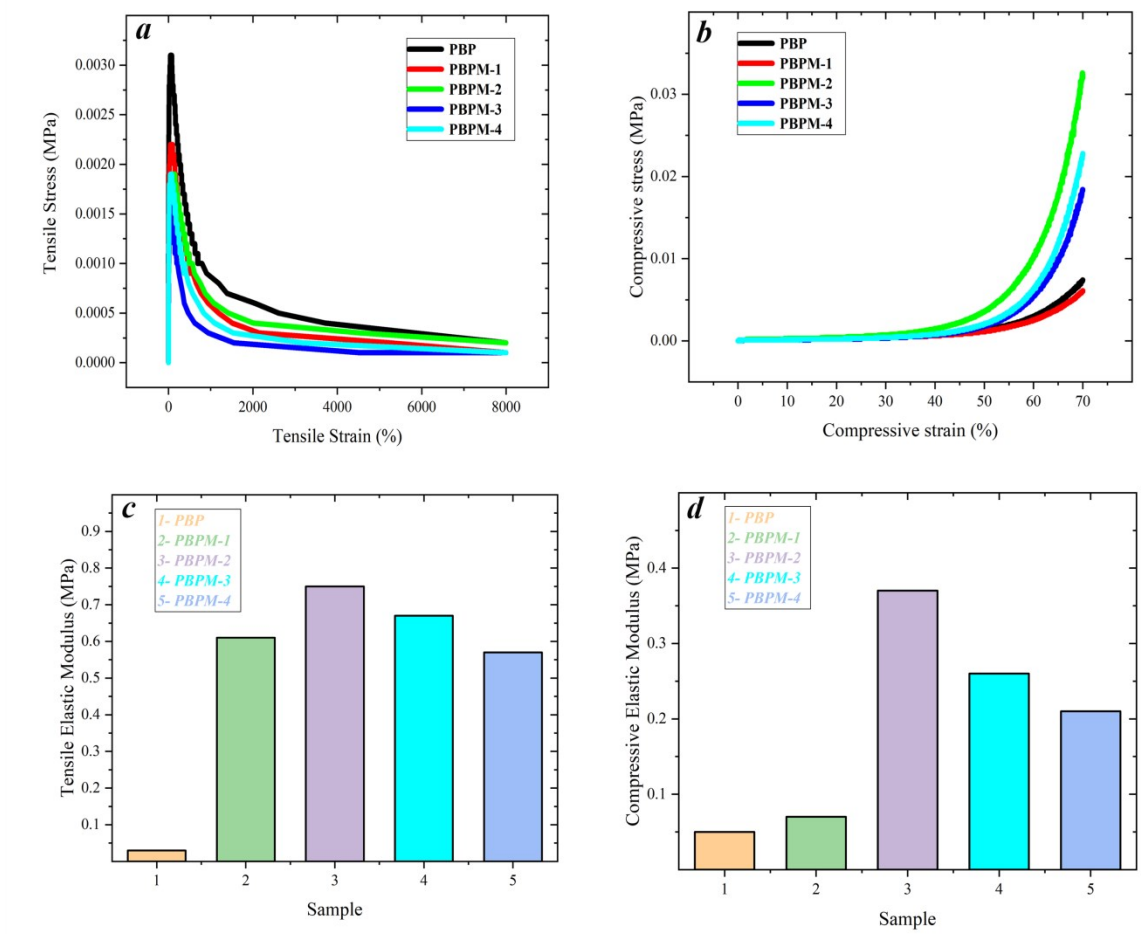

Figure S4. Stress-strain experiments to quantitatively analyze the impact of composition on the performance. (a) Tensile stress-strain curves of the hydrogels with different MXene contents. (b) Compressive stress-strain curves of the hydrogels with different MXene contents at 0-70% strain. Histograms of (c) tensile and (d) compressive elastic modulus of the hydrogels with different MXene contents.

Figure S5. Excellent mechanical properties of the PBPM-2 hydrogel: (a) original state of the PBPM-2 hydrogel; (b) flexural and (c) helical twisting state of the PBPM-2 hydrogel.

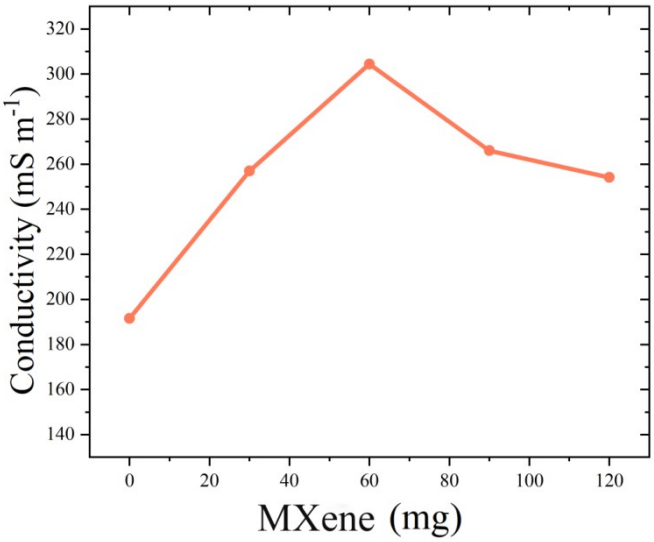

Figure S6. Conductivity variations for the hydrogels with different MXene contents.

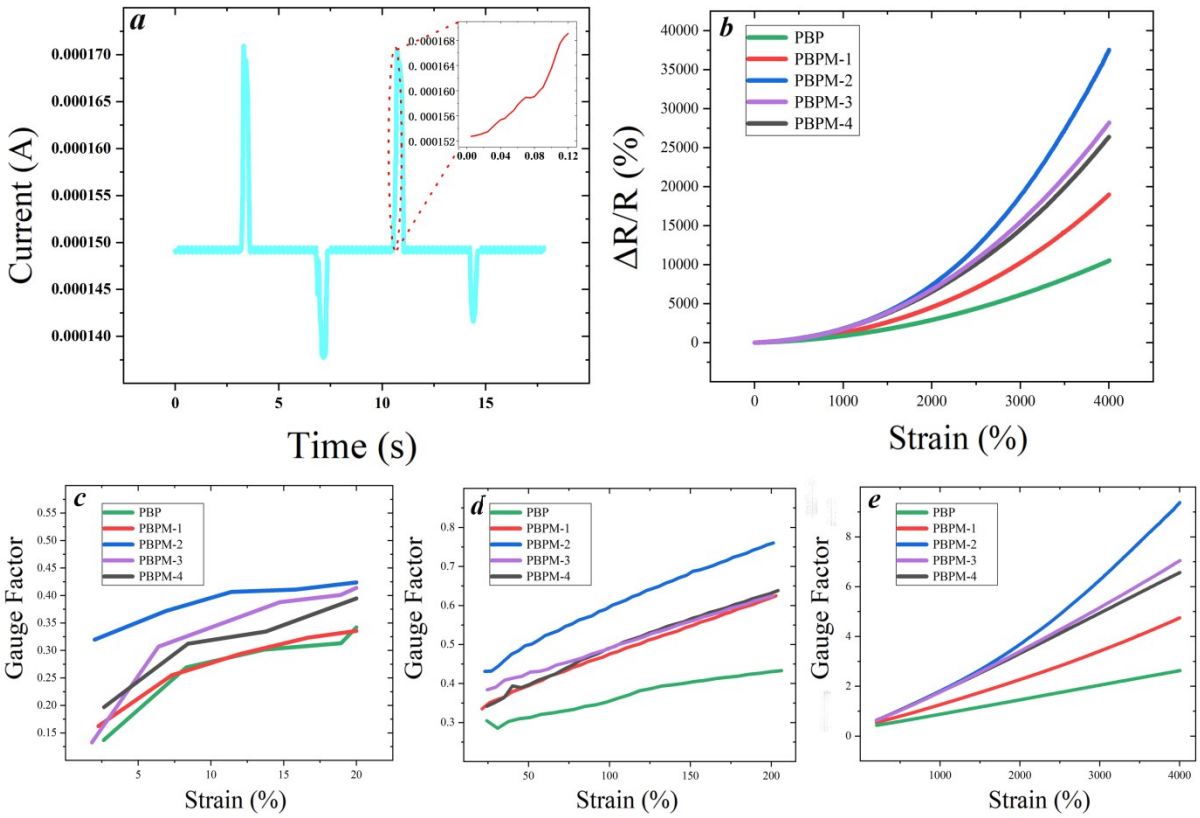

Figure S7. Strain sensing performances of the hydrogels. (a) Real-time current response of the PBPM-2 hydrogel. Inset shows the response time. (b) Variations of relative resistance change ($\Delta R/R_0$) of the hydrogels at 0-4000% strain. (c-e) Variations of gauge factor (GF) of the hydrogels at different strains of 0-20%, 20-400%, 200-4000%.

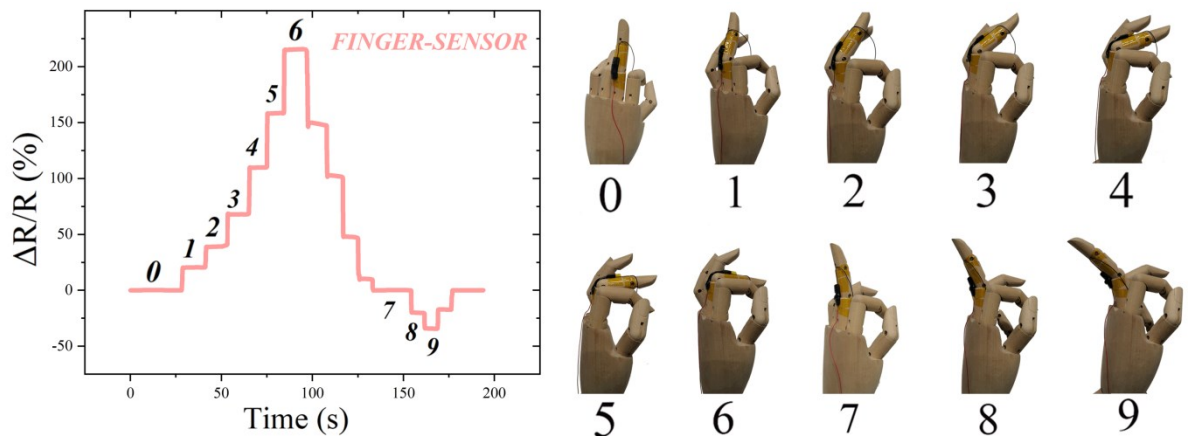

Figure S8. PBPM-2 hydrogel as flexible electronic skin finger sensor to detect different angles and directions.

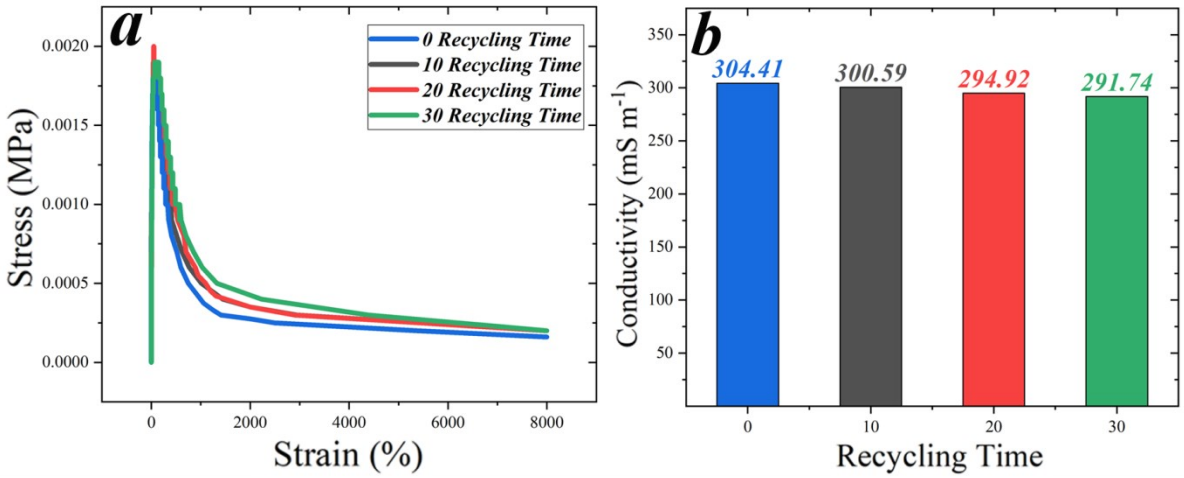

Figure S9. Mechanical tensile and conductive properties of the PBPM-2 hydrogel recycled for different times. (a) Stress-strain curves and (b) conductivity change with different recycling times.

Table S1. Comparison of the self-healing efficiency, self-healing time and direction-aware ability between the PBPM-2 hydrogel and other hydrogels reported in the literatures.

Hydrogel	Self-healing efficiency*	Self-healing Time	Direction-aware ability	Reference
MXene-hydrophobically associated polyacrylamide/poly(N-isopropyl acrylamide)	59.5%	72 h	No	[1]
Poly(1,4-cyclohexanedimethanol succinate-co-citrate)	97.0%	30 s	No	[2]
Polymer/microgel complex coacervate	92.0%	24 h	No	[3]
Clay/poly(2-(2-methoxyethoxy) ethyl methacrylate-co-oligo (ethylene glycol) methacrylate)	84.8%	12 h	No	[4]
Agarose/poly(vinyl alcohol)	90.0%	10 s	No	[5]
Polyborosiloxane /polydimethylsiloxane	86%	6 h	No	[6]
Dopamine-coated reduced-graphene oxide/hydroxypropyl guar gum	90.5%	2 h	No	[7]
Functionalized single-wall carbon nanotube/polydopamine-polyvinyl alcohol	99.0%	2 s	No	[8]
Poly((3-sulfopropyl methacrylate potassium salt-r-methyl methacrylate)	98.3%	3 h	No	[9]
Cellulose nanocrystals /cellulose nanofiber-polypyrrole/polyvinyl alcohol	72.0−76.3%	30 min	No	[10]
Gelatin/polyacrylamide/acrylated dopamine-Fe^{3+}	90.0%	24 h	No	[11]
Alginate-gelatin/polypyrrole	40.0%	2 h	No	[12]
PBPM-2	100%	0.06 s	Yes	this work

Note:* indicates the percentage of original tensile strength recovered.

Table S2. Components of the PBPM hydrogels.

Hydrogel	**PVA (g)**	**Bn (g)**	**PEI (g)**	**MXene (g)**
PBP	0.6	0.09	0.6	/
PBPM-1	0.6	0.09	0.6	0.03
PBPM-2	0.6	0.09	0.6	0.06
PBPM-3	0.6	0.09	0.6	0.09
PBPM-4	0.6	0.09	0.6	0.12

References

1. Y. Zhang, K. Chen, Y. Li, J. Lan, B. Yan, L. Y. Shi and R. Ran, *ACS Appl. Mater. Interfaces*, 2019, **11**, 47350-47357.
2. J. H. Yoon, S. M. Kim, Y. Eom, J. M. Koo, H. W. Cho, T. J. Lee, K. G. Lee, H. J. Park, Y. K. Kim, H. J. Yoo, S. Y. Hwang, J. Park and B. G. Choi, *ACS Appl. Mater. Interfaces*, 2019, **11**, 46165-46175.
3. S. Wu, M. Zhu, D. Lu, A. H. Milani, Q. Lian, L. A. Fielding, B. R. Saunders, M. J. Derry, S. P. Armes, D. Adlam and J. A. Hoyland, *Chem. Sci.*, 2019, **10**, 8832-8839.
4. P. Wei, T. Chen, G. Chen, H. Liu, I. T. Mugaanire, K. Hou and M. F. Zhu, *ACS Appl. Mater. Interfaces*, 2019, **12**, 3068-3079.
5. M. S. Tsai, T. L. Shen, H. M. Wu, Y. M. Liao, Y. K. Liao, W. Y. Lee, H. C. Kuo, Y. C. Lai and Y. F. Chen, *ACS Appl. Mater. Interfaces*, 2020, **12**, 9755-9765.
6. M. Tang, P. Zheng, K. Wang, Y. Qin, Y. Jiang, Y. Cheng, Z. Li and L. Wu, *J. Mater. Chem. A*, 2019, **7**, 27278-27288.
7. Z. Sun, L. Wang, X. Jiang, L. Bai, W. Wang, H. Chen, L. Yang, H. Yang and D. Wei, *Int. J. Biol. Macromol.*, 2019, **155**, 1569-1577.
8. M. Liao, P. Wan, J. Wen, M. Gong, X. Wu, Y. Wang, R. Shi and L. Zhang, *Adv. Funct. Mater.*, 2017, **27**, 1703852-1703862.
9. J. Lee, M. W. M. Tan, K. Parida, G. Thangavel, S. A. Park, T. Park and P. S. Lee, *Adv. Mater.*, 2019, **32**, 1906679-1906688.
10. L. Han, S. Cui, H. Y. Yu, M. Song, H. Zhang, N. Grishkewich, C. Huang, D. Kim and K. M. C. Tam, *ACS Appl. Mater. Interfaces*, 2019, **11**, 44642-44651.
11. Z. Gao, Y. Li, X. Shang, W. Hu, G. Gao and L. Duan, *Mater. Sci. Eng. C*, 2020, **106**, 110168-110168.
12. K. Ren, Y. Cheng, C. Huang, R. Chen, Z. Wang and J. Wei, *J Mater. Chem. B*, 2019, **7**, 5704-5712.